Collective dynamics on a crystal composed by disparate-mass particles: $Li_{22}Pb_5$

R. Fernández-Perea,[1,*] F.J. Bermejo,[1] J.L. Martínez,[1] E. Enciso,[1] and P. Verkerk[2]
[1]*Consejo Superior de Investigaciones Científicas, Serrano 123, Madrid E-28006, Spain*
[2]*Interfacultair Reactor Instituut, TU Delft, 2629 JB Delft, The Netherlands*
(Received 20 October 1998)

The lattice dynamics of crystalline $Li_{22}Pb_5$ is studied by means of computer simulations. The calculated spectrum shows several bands corresponding to modes in which only the light atoms execute motions. The spectrum of acoustic modes is found to be well separated from the high-frequency bands and is in all cases confined to frequencies below 4 meV. The results are shown to provide a clue for the understanding of the origin of the strong anomalous dispersion features found in the melt by experiment [Phys. Rev. Lett. **80**, 2141 (1998)] and molecular dynamics simulations [Phys. Rev. E **58**, 4568 (1998)]. [S1063-651X(99)10003-5]

PACS number(s): 62.60.+v, 63.50.+x, 62.65.+k

I. INTRODUCTION

The neutron-scattering response of a harmonic lattice in which a small concentration of atoms have masses different from the rest can be calculated in closed form [1]. The resulting spectrum shows marked departures from that of the pure lattice. To start with, a contribution of diffuse-scattering origin due to disorder brought forward by the ''impurities'' becomes noticeable. Concomitantly, the coherent cross section will show peaks at frequencies shifted and substantially broadened with respect to those of the native crystal. Some of these shifts may be exceptionally large and are thought to correspond to normal modes showing vibration amplitudes which decay faster than exponentially with increasing distance from the defect. Finally, for finite (above a few percent) defect concentrations a band of localized modes is expected to appear, the width of which is dependent upon the defect concentration [2].

The predictive power of the treatments just referred to is, however, limited. The comparison of the predictions with experimental data on rubidium-potassium alloys [3] is a classic in the field. It shows that although the theory predicts the presence of two peaks in the spectrum arising from the phonons as well as from the localized (defect) modes, their position and widths exhibit marked disagreements with the prediction as soon as the concentration of the defect (potassium) particle rises above some 6%.

Here, our main motivation is to understand the spectrum of the spontaneous fluctuations [i.e., the generalized susceptibility $\chi(Q,E)$, where Q stands for momentum transfer and E for frequency, or energy transfer] in the density of a disordered alloy, where the concentration of defects is well above the limit referred to above. The interest in such a study grew from previous experience on the dynamics of molten metallic alloys such as Li_4Pb [4,5], rather than from an explicit need to delve into the dynamics of defects, as such. In fact, the system noted above is a very convenient realization of a fluid consisting of disparate-mass particles previously analyzed by kinetic theory [6]. The theoretical expectancy is that at wave vectors well beyond the hydrodynamic realm, the spectrum is dominated by two ''kinetic modes'' the frequencies of which substantially depart from those given by an extrapolation to larger wave vectors of hydrodynamic sound having frequencies given by the linear dispersion law $\omega_s = c_s Q$ in terms of the adiabatic sound velocity c_s.

The presence of a spectral band showing an apparently high anomalous dispersion has been proven by experiments [4,7], and the main features of the spectra are now understood on the basis of computer molecular dynamics simulations carried down to scales where the two ''kinetic modes'' merge with that corresponding to hydrodynamic sound [5]. Since the same ''kinetic modes'' which appear in the fluid mixture are expected to show up if the system is frozen into its crystalline ground state [6], evaluation of the spectral shape of the crystal spectrum and its understanding in terms of well defined frequencies and eigenvectors seems now a must. Indeed, contrary to what is the case in the liquid, finite-lifetime effects due to phonon damping can be reduced to a minimum, the discussion of whether a ''mode'' propagates or not can be put on a quantitative basis since now the wave vector **Q** becomes a good ''quantum number'' enabling the dynamics to be accounted for in terms of a few normal modes (i.e., the microscopic dynamics is describable by a number of excitations which is very small if compared with the number of particles composing the condensed body), and, last but not least, information about the character of the different spectral bands can be established unambiguously by examination of the mode eigenvectors.

II. COMPUTATIONAL DETAILS

In what follows we describe the results of a computer simulation study on a model for the crystal which is stoichiometrically closest to Li_4Pb, which is $Li_{22}Pb_5$ [8]. A glance to the phase diagram of the phases formed between lithium and lead [9] shows the existence of five intermetallic compounds LiPb, Li_5Pb_2, Li_3Pb, Li_7Pb_2, and ''Li_4Pb.'' The latter phase, although stable within the liquid, undergoes a phase separation if frozen rapidly. Indeed, the closest crystalline composition to that of the A_4B octet was found to be that of $Li_{22}Pb_5$ [8] (a difference of about 1.5% in composition with Li_4Pb).

*Present address: Argonne National Laboratory, Argonne, IL 60439.

Experimental x-ray diffraction from a single crystal of $Li_{22}Pb_5$ [8] showed that the unit cell contains 432 atoms on a face-centered cube of side $a=20.08$ Å at room temperature, corresponding to a density of 3.88 g cm^{-3}. This large cell volume accommodates 16 formula units, that is, 80 Pb and 352 Li atoms. The space group was assigned as $F23$ (Patterson symmetry $Fm\bar{3}$), and as a characteristic feature it shows that the unit cell can be decomposed into 216 subcells ($6\times6\times6$) of two atoms each. Such a pattern shows an approximate body-centered-cubic structure with a cell constant roughly 1/6 of a which seems common to other Li-Pb intermetallic compounds [10]. The idealized structure then corresponds to a coordination of eight nearest neighbors for each Pb atom and each Li is surrounded by another eight of which three or fewer are Pb. (Some deviations from the idealized structure concerning the positions of Pb are reported in the original article [8]. Those for Li could not be ascertained because of its low contrast for x rays.)

The computer simulation was carried out on a crystal structure generated from the atomic parameters and symmetry operations given in Ref. [8].

The effective potential used for the simulations was the same used previously for the analysis of the liquid dynamics [5]. It corresponds to the model of Copestake *et al.* [11], which reads

$$V_{ij}(r)=k_BT\ a\exp[(d-r)/p]+Q_iQ_je^2\exp[-\lambda r]/r, \quad (1)$$

with interaction parameters set to values given in Ref. [12]. Both a and p serve to soften the repulsive core (assumed to be equal for all atoms), the latter given in terms of a hard-core diameter $d=2.0$ Å. The second term sets the chemical interactions between the particles constituting the alloy. For such a purpose, negative and positive charges eQ resulting from the strong charge-transfer effects known to take place are set to lead and lithium atoms, respectively, while total charge neutrality is maintained [11]. Finally, the exponential in the second term accounts for screening effects from metallic electrons, which are quantified in terms of the parameter $\lambda=4\pi e^2N(E_F)$, which in turn is given by the value of the electronic density of states at the Fermi level.

Once the simulation box was set up the temperature was decreased down to 1 K and the structure was left to relax. The structure was then left to stabilize and several static and dynamic quantities were calculated afterwards. Figure 1 displays the $g_{\alpha\beta}(r)$ partial pair radial distribution functions which specify the distribution of the different atomic species up to 10 Å. An estimate of the coordination numbers is provided by the integrals $\int_0^{r1}dr4\pi r^2g_{\alpha\beta}(r)$, which are taken over limits established by well defined peaks in the $g_{\alpha\beta}(r)$ functions. The relevant numbers are ≈7.9 Li atoms around each Pb and ≈1.8 Pb atoms surrounding each lithium. In other words, the result shows that the crystal structure is fairly stable with respect to the interaction potential. Raising the temperature up to 64 K has a minor effect on the coordination numbers, which are altered by less than 3%.

The computation of dynamic properties at such a low temperature (1 K) was found to be severely limited by the statistical accuracy achievable in reasonable computer time (atomic motions are too infrequent that an unaffordable large number of trajectories would need to be calculated). To improve this, the temperature was raised stepwise and allowed to stabilize at several discrete values (2, 4, 8, 16, 32, and 64 K). The crystal structure was in all cases stable (no traces of diffusive atomic motions were found in the calculated density of states). Most of the calculations thus refer to this last temperature $T=64$ K, although some results for $T=1$ K will also be discussed, mainly for comparison purposes. The temperature of 64 K that was chosen represented a tradeoff between statistical accuracy and some broadening of the spectra and static distributions. A comparison between the $g_{\alpha\beta}(r)$ functions and those measured at lower temperature is also provided by Fig. 1. There it is seen that the main effect concerns a broadening of all peaks arising from thermal motions. Also, a comparison of the local structure of the crystal with that of liquid Li_4Pb [5] can easily be gauged from the figure.

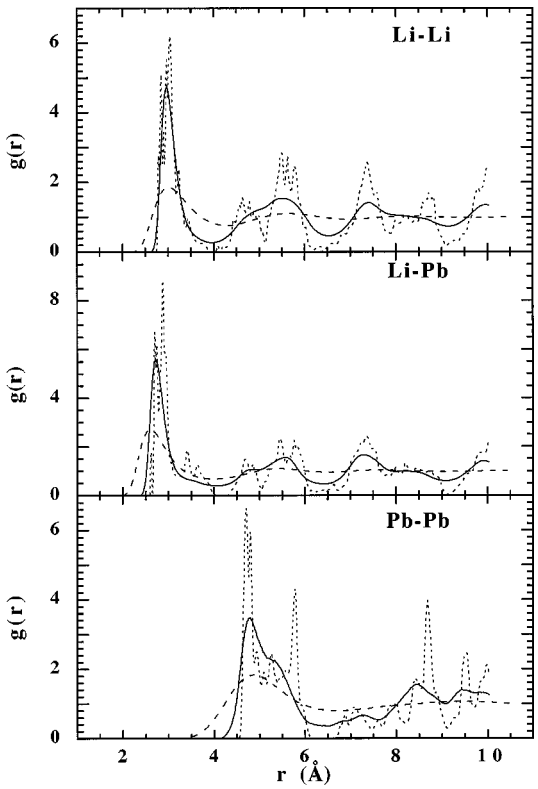

FIG. 1. Calculated partial radial distribution functions for the crystal at $T=1$ K (dots), at 64 K (solid), and for the melt at 1075 K (dashes).

For a crystal partially composed of relatively light particles such as ^{7}Li, quantum interference effects may be expected to be important at low temperatures. To ascertain whether such effects need to be considered at the temperature under consideration, we have evaluated the thermal de Broglie wavelength $\Lambda=(2\pi\hbar^2/k_BTM_{\mathrm{Li}})$ for ^{7}Li at 64 K. The result yields a wavelength of about 0.8 Å, which is well below the shortest distances (≈3 Å) and thus justifies the use of fully classical grounds in the study of the dynamics.

More than 400 simulation runs were made over 0.25 ns employing a time step of 5 fs to get enough statistics to enable the calculation of the relevant quantities which followed well established procedures.

To facilitate comparison with experiment the dynamical

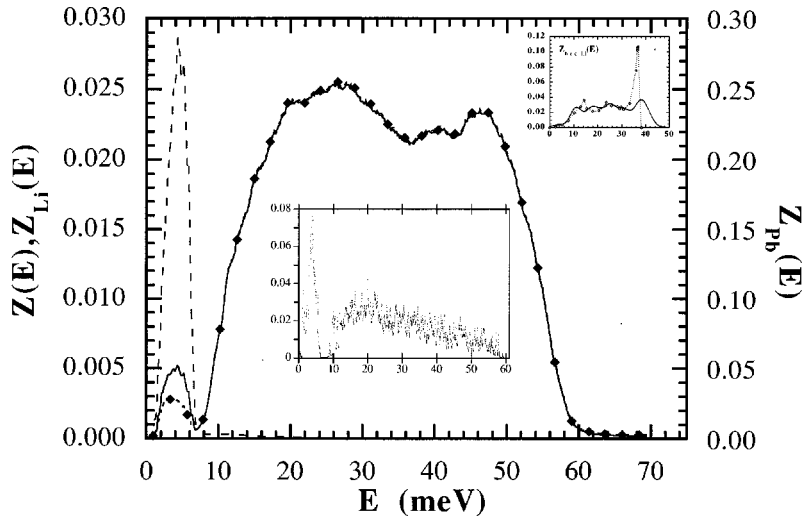

FIG. 2. Generalized frequency spectra as calculated from the Fourier transforms of the atomic velocity autocorrelation functions for the Li atoms (dashed line with lozenges), for Pb atoms (dashes), and the total (average) frequency distribution (solid line). The inset below the main curve shows the calculated quantity for $T=1$ K. That in the upper right corner compares the frequency distribution as calculated for pure Li metal using the present potential (solid line) with the experimental estimate of Ref. [13].

quantities have been weighted by the thermal neutron scattering lengths, $\overline{b}_{\mathrm{Li}}=-0.229$ fm, $\overline{b}_{\mathrm{Pb}}=0.94$ fm.

III. RESULTS

A. Single-particle properties

The most basic quantity to describe the microscopic dynamics of a condensed body is the $Z(E)$ generalized frequency spectrum (vibrational density of states) which is related via a Fourier transform to the atomic velocity autocorrelation functions for the individual particles. Our calculated $Z(E)$ functions for the average atom within the crystal as well as those of $Z_{\mathrm{Li,Pb}}(E)$ for the individual Li and Pb species are shown in Fig. 2. As expected, most of the frequency spectrum for the heavy (Pb) particles is confined below 10 meV. In contrast, that for the light component stretches up to 60 meV and shows a fairly structured shape. At least three maxima are visible at about 25 meV, 40 meV, and 46 meV, which correspond to frequencies where the ''fast mode'' could be followed experimentally in the liquid [4,7]. The appearance of an additional very well defined peak at 3 meV $Z_{\mathrm{Li}}(E)$, that is, at frequencies comparable to those where $Z_{\mathrm{Pb}}(E)$ shows its maximum, is here of special relevance. First, it shows that *both light and heavy* particles move with the same frequencies in this range of the spectrum, and second, the fact that such a low-frequency peak in $Z_{\mathrm{Li}}(E)$ is well separated from the rest of the distribution serves to put some bounds to the maximum frequencies reachable by the acoustic phonon branches [in actual fact there exists a gap in $Z(E)$ which becomes far wider at lower temperatures].

A comparison of the $Z(E)$ for $T=64$ K with that calculated at $T=1$ K is also enabled by the graph drawn in the inset of Fig. 2. The structure of the latter quantity is the same as that for higher temperature, showing a peak below 6 meV and a broad band stretching up to 60 meV. The intensity ratio of the two peaks departs from that found at higher temperature, an effect which can possibly be ascribed to the strong anharmonicity built in in the Li interaction potential. In actual fact, a softening of the force constants as large as 10% going from 100 K to 293 K was reported from an experimental study on crystalline lithium [13]. At any rate, the important qualification to be made from such a comparison is that the width of the high-frequency band remains basically the same between 1 K and 64 K and therefore cannot be attributed to effects brought forward by thermal motions.

The frequency distribution can also be compared with that calculated for the liquid at 1075 K shown in [5]. The extent of frequencies covered by the distribution is in both cases basically the same. The strong quasielastic component characteristic of the liquid obviously made it impossible to reveal the presence within the melt of the low-frequency peak seen in the crystalline $Z_{\mathrm{Li}}(E)$.

A point also worth noting concerns the frequency range of the spectrum, which far exceeds that of pure Li. In fact, the density of vibrational states of crystalline ^{7}Li as measured by neutron scattering [13] is confined to frequencies below 40 meV (see inset in Fig. 2). To ascertain whether the presence of such high frequencies occurs as an artifact of the simulation, several calculations were carried out for a Li bcc crystal using a cell constant of 3.48 Å and the Li-Li interaction potential. The resulting crystal structure was found to be stable for this potential up to $T=200$ K at least. The calculated $Z(E)$ consists of a spectrum showing the six singularities commensurable with the crystal structure and is confined to frequencies below 50 meV as shown in the inset of Fig. 2. This cutoff frequency comes some 20% above experiment but is definitely lower than that of the alloy, which stretches up to 60 meV. Such high frequencies can be assigned to vibrations of Li-Pb pairs which occur as a consequence of the strong short-range forces built in within the ordering potential [14]. In fact, an effective force constant $k^{\mathrm{eff}}_{\mathrm{LiPb}}=64.3$ N/m is derived from the peak frequency which compares with the value of $k_{\mathrm{LiPb}}=10.09$ N/m computed for an isolated Li-Pb atom pair from the second derivative of the

interaction potential at the equilibrium distance. Such estimates are about one order of magnitude larger than the stiffest force constant in pure crystalline Li [13] and thus serve to explain the stretching of the frequency spectrum up to such high frequencies.

The appearance in $Z_{\mathrm{Li}}(E)$ of bands at frequencies which are both well below and above those of pure lithium is reminiscent of the behavior of heavy interstitials on cubic metals [15]. There, such a phenomenon is understood on the basis of the high compressions found for the lattice surrounding the defect. Even if the analogy cannot be followed in full to the present case, our finding can be rationalized on the basis of the large value of the k_{LiPb} referred to above. From there, one could expect the appearance of localized high-frequency modes having frequencies ω_L considerably higher than the highest cutoff in the spectrum of the pure metal. These high-frequency vibrations would involve stretching the Li-Pb bonds considerably. Concomitantly, ''resonant'' modes involving slight stresses of such bonds are expected to show at frequencies well below the lowest singularity in the spectrum of the pure metal.

The atomic mean-square displacements $\langle r^2(t)\rangle$ were examined in some detail. The amplitude of motion for both Li and Pb was found to be fairly comparable, the main difference being in the far higher frequency exhibited by motions of the light particle. Such closeness of the vibration amplitudes of Li and Pb (expected for a perfectly harmonic lattice only) seems to point to an enhancement of the displacements of the heavy particle, much akin to those found for dilute heavy impurities giving rise to *resonant* modes [15]. A computationally convenient estimate of the deviation of the atomic motions from ideal (harmonic and isotropic) behavior is provided by the calculation of the coefficients $\alpha_n(t)$ which appear in the cumulant expansion of the $F_s(Q,t)$ intermediate self-scattering function [16] [the transform of $G_s(\mathbf{r},t) = \Sigma_j\langle \delta(\mathbf{r}-R_0(t)+\mathbf{R}_0)\rangle$ which is the self-pair-correlation or van Hove function, giving the probability that a particle at the origin at time $t=0$ is at $\mathbf{r}$ at time t]. These are defined as [16]

$$\alpha_n(t)=\frac{\langle r^{2n}(t)\rangle}{c_n\langle r^2(t)\rangle^n}-1,\quad c_n=\frac{1\times 3\times 5\times\cdots\times(2n+1)}{3^n}. \quad (2)$$

Such coefficients, which are related to the mean-square atomic displacements and thus to the moments of $G_s(\mathbf{r},t)$ [in fact they are just $\int d\mathbf{r} r^2 G_s(\mathbf{r},t)$], are defined to vanish when the $G_s(\mathbf{r},t)$ is a Gaussian, that is, when atomic motions take place within a harmonic and isotropic potential. Negative values for such parameters are indicative of a time decay faster than Gaussian, and the converse otherwise. The values found for $\alpha_{n=2,3,4}(t)$ are -0.37 (7), 12 (4), and 34 (25) for motions involving Pb and -0.33 (5), 15 (5), and 54 (49) for those concerning Li. In other words, even at such relatively low temperature, both types of atoms exhibit noticeable anharmonic and/or anisotropic behavior in their motions. The point seems to be of interest, since, as stated in the Introduction, one would expect a behavior like this to be followed by the ''defect'' particles only.

B. Collective dynamics: Spatial dependence of the excitations

Our exploration of the $[\mathbf{Q},E]$ plane will here be limited to higher-symmetry $[\zeta 00]$, $[\zeta\zeta 0]$, and $[\zeta\zeta\zeta]$ directions. As we shall describe, the simulation cell allows us to reach as the minimum wave vector the value $2\pi/a(1,0,0)=0.312$ Å^{-1}, although lower values are allowed by the crystalline symmetry. In what follows and in order to make contact with previous simulation and experiment on the molten alloy use is made of absolute units for the $\mathbf{Q}$ wave vector, rather than the usual units reduced by the lattice constant. Also, most of the wave-vector-dependent quantities will here be plotted as

$$J_{\mathrm{l}}(\mathbf{Q},E)=E^2S(\mathbf{Q},E), \quad (3)$$

which for an isotropic body such as a liquid become the longitudinal current-current correlations,

$$J_l(Q,E)=\frac{E^2}{Q^2}S(Q,E)=\frac{E^2}{Q^2}\sum_{\alpha\beta} b_\alpha b_\beta S_{\alpha\beta}(Q,E), \quad (4)$$

which are often used in liquid-state physics to display experimental or computer-simulation results. Here, $\overline{b_{\alpha,\beta}}$ stands for the scattering lengths of both types of nuclei and $S_{\alpha\beta}(Q,E)$ specifies the dynamic correlations between the density of species α and that of species β, i.e., it is the Fourier transform of the time correlation function $\langle \rho_\alpha(Q,t)\rho_\beta(Q,0)\rangle$ of the particle density $\rho(Q,t)$.

A set of representative spectra plotted in terms of $J_l(\mathbf{Q},E)$ is shown in Fig. 3 for the three crystal higher-symmetry directions. In all cases the range of wave vectors explored stretches from about one-half to the Brillouin zone boundaries. A first glance at the curves drawn in Fig. 3 reveals that spectra at such reciprocal-lattice vectors are composed of a narrow band below ≈8 meV showing a multiplet structure if examined on a narrower frequency scale, and a broader (widths of ≈5 meV or larger), higher-frequency component with maxima located at widely different frequencies, dependent upon the specific direction. Such frequencies show a remarkably strong anisotropy as can be gauged from their variation at the zone boundaries which goes from ≈35 meV along $[\zeta 00]$ and ≈48 meV for $[\zeta\zeta\zeta]$. In all cases, a fairly complicated spectral pattern develops between the referred two points within each of the crystal directions. Such a large number of spectral peaks arises as a consequence of the intricate atomic dynamics taking place within such a complicated unit-cell structure which, as will be mentioned below, shows some local deviations from the idealized $F23$ cubic structure.

Examination of the wave-vector dependence of the spectral shape shows that whereas the low-frequency bands experience relatively small changes as $|\mathbf{Q}|$ increases, at least four different bands become visible at high frequencies. If we now spend some time following the evolution of the amplitudes of the main peaks, we make the following observations: (a) the intensity of the low-frequency peak increases monotonously with increasing $|\mathbf{Q}|$ up to the wave vector where the structure factor shows a Bragg peak (1.25 Å^{-1}, 2.09 Å^{-1}, and 1.04 Å^{-1} for $\langle\zeta 00\rangle$,$\langle\zeta\zeta 0\rangle$, and $\langle\zeta\zeta\zeta\rangle$ directions, respectively), (b) the amplitude of the strong, high-frequency band seen at wave vectors about one-half up to the

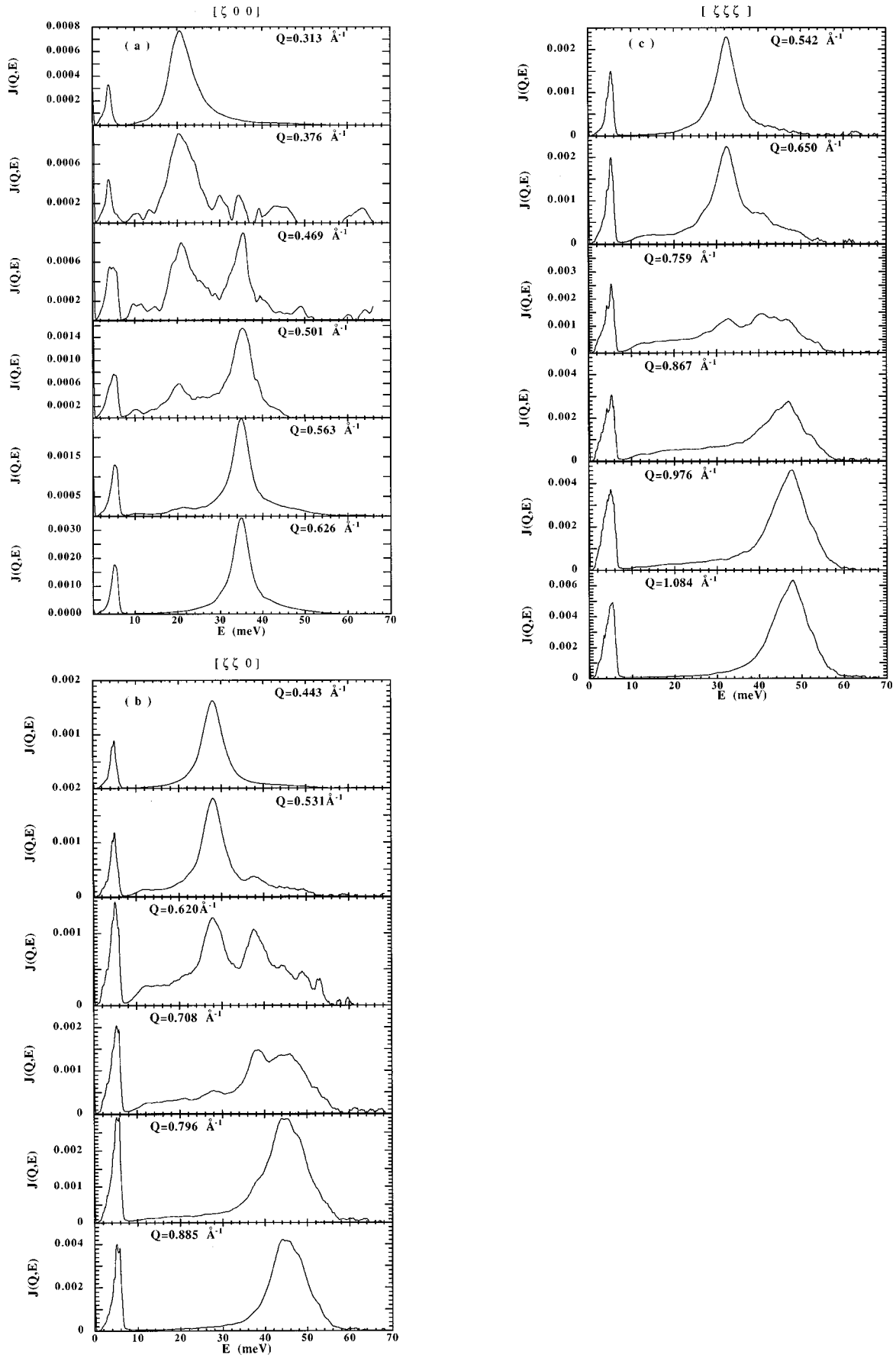

FIG. 3. A representative sample of $J_I(\mathbf{Q},\mathrm{E})$ spectra corresponding to directions (a) $[\zeta 00]$, (b) $[\zeta\zeta 0]$, and (c) $[\zeta\zeta\zeta]$. The corresponding momentum transfers are shown as insets.

zone edge decreases with increasing $|\mathbf{Q}|$ and the peak seems to show a vanishing intensity at the zone boundary, (c) the amplitude of the peaks which develop at both sides of the main band shows a complicated pattern; that appearing at the higher-frequency edge being the one which dominates the spectrum of high frequencies at the zone boundary. In other words, rather than showing a strong dispersive behavior, the higher- frequency bands show intensity patterns commensurate with excitations of purely ''optical'' character which would correspond to atomic motions rather weakly coupled to the low-frequency acoustic phonons. The latter become visible only at a few special wave vectors ($Q \approx 0.1$–0.2 Å^{-1}) and appear as weak but dispersive peaks at frequencies of the order of 1–2 meV which are located in the trailing end of the intense band centered at about 5 meV. Such a dispersion corresponds to a hydrodynamic sound velocity of about 2500 m s^{-1}, a figure some 300 m/s above the estimate found for the Li_4Pb melt. Following in more detail the dispersion relations across the Brillouin zone is hampered by the presence of peaks within frequencies of 4–6 meV which show characteristics compatible with those of low-frequency optic branches (i.e., crossing the acoustic dispersions with frequencies well below those reachable by the acoustic branches at the zone edge).

From the spectra shown in Fig. 3 some conclusions can be drawn, at least on qualitative grounds. The first concerns the dominant character of the low- and high-frequency parts of the spectra. The fact that the former closely follows the Q dependence of the structure factor provides a clear indication of the dominant (but presumably not exclusive) acoustic character for this band. On the other hand, the band which appears at frequencies between $\approx$20 meV [$\zeta 00$] and $\approx$32 meV [$\zeta\zeta\zeta$] shows an intensity pattern corresponding to an excitation of purely ''optical'' origin, as seen from its intensity, which becomes maximal at some point within the first Brillouin zone and vanishes at the zone boundary. The other peaks arise from the complicated dynamics within such a large unit cell. In this respect, one could think about having a minimum number of six branches corresponding to the decomposition of the unit cell in terms of the $6\times6\times6$ cells of two atoms each, as mentioned above. On the other hand, from the coordination found in the idealized structure one would expect to find fairly flat optical branches since interactions within each subcell (especially those involving Li-Pb contacts) are certainly far stronger than those between cells.

In close parallel with what was found for the melt, the width of the high-frequency spectra is found to be far larger than that corresponding to the pure Li metal [5]. In fact, a rather well defined collective mode which corresponds to a continuation within the kinetic realm of the hydrodynamic sound mode (dubbed an ''extended sound mode'' in the terminology of Campa and Cohen [6,17]) is found for the pure molten metal by simulation [5] and experiment [18]. In contrast, only very short-lived (less than 1 ps) excitations are found when the metal is embedded in the alloy [4]. The remark is of interest since it points to a strong lifetime effect carried forward by the presence of the heavy particles. As a matter of fact, the finding found here for the crystal is commensurate with the very short lifetime of the excitations found experimentally in the melt [4]. Such a characteristic seems to be in common with the ''impurity band'' found for large concentrations of mass defects in binary crystals (compare the result with that of Ref. [3] for a concentration of light particles of 0.26). Furthermore (keeping in mind the difficulties in calculating low-temperature spectra since very few lattice points yielded statistically significant spectra at 1 K), the observed widths at $T=64$ K are not larger than those computed for $T=1$ K by a substantial amount. In other words, the observed widths can surely be attributed to the presence within the Li matrix of the Pb atoms which act as ''trapping centers'' for any propagating excitation.

To investigate on a more quantitative basis the relaxation of this high-frequency mode we have also evaluated the participation ratio as well as the kinetic-energy partial autocorrelation functions which for a body composed by $N_{i=\alpha,\beta}$ particles moving with velocities v_i are defined as [19]

$$P_\alpha^{-1}=\frac{N_\alpha \sum_{j=1}^{N_\alpha} v_j^4}{\left(\sum_{j=1}^{N_\alpha} v_j^2\right)^2}, \quad h_{\alpha\beta}(r)=\frac{\sum_{j,k=1}^{N_\alpha N_\beta} v_j^2 v_k^2 \delta(r-r_{jk})}{\sum_{j,k=1}^{N_\alpha N_\beta} \delta(r-r_{jk})}. \quad (5)$$

P_α would yield values of about 1 for a mode in which all atoms participate and a figure down to $1/N_\alpha$ for ''localized'' modes. The behavior expected for $h(r)$ for a mode extended over the crystal volume would be a constant value showing some superimposed oscillations arising from the sum of the δ terms which basically represent the static-pair-correlation functions. Conversely, a mode confined to a spatial domain will give rise to an $h(r)$ function which decays with distance, indicating that the kinetic energy is contained in few atoms.

The obtained result for P [sum in Eq. (5) over all particles] came as a surprise since it gives a participation ratio indicating that, on average, about only one-half of the atoms participate in the high-frequency motions. Specifically, the value found for the average atom within the sample came out quite close to 0.5, whereas P_{Li} and P_{Pb} yielded 0.61 and about 0.59, respectively. On the other hand, as shown in Fig. 4, the $h_{\alpha\beta}(r)$ partial autocorrelations show a flat behavior with r giving an average value which obviously depends on the atomic species, over which a marked modulation is superimposed. A comparison of the location of peaks in $h_{\alpha\beta}(r)$ with the spatial structure of the crystal as defined by the partial static correlations $g_{\alpha\beta}(r)$ depicted in Fig. 1 indicates that extrema in $h_{\alpha\beta}(r)$ correspond to peaks and valleys in the partial pair correlations. Peaks above the average level in $h_{\alpha\beta}(r)$ are found for distances corresponding to maxima in the relevant $g_{\alpha\beta}(r)$ and the converse applies to those below the average values. Also, it seems worth noting that the structure shown by graphs in Fig. 4 appears to be closer to that of the $g_{\alpha\beta}(r)$ functions of the crystal at 1 K than to those of that at 64 K actually used for the calculation. This can easily be understood if one recalls that $h(r)$ will be dominated by the largest velocities and that these in turn correspond to those of oscillating atoms when passing through their equilibrium positions (potential minima). As the crystal structure does not change considerably with temperature [i.e., the positions of the main peaks in $g(r)$ do not shift between 1 K and 64 K], one expects that atoms displaced far from equilibrium positions will hardly contribute

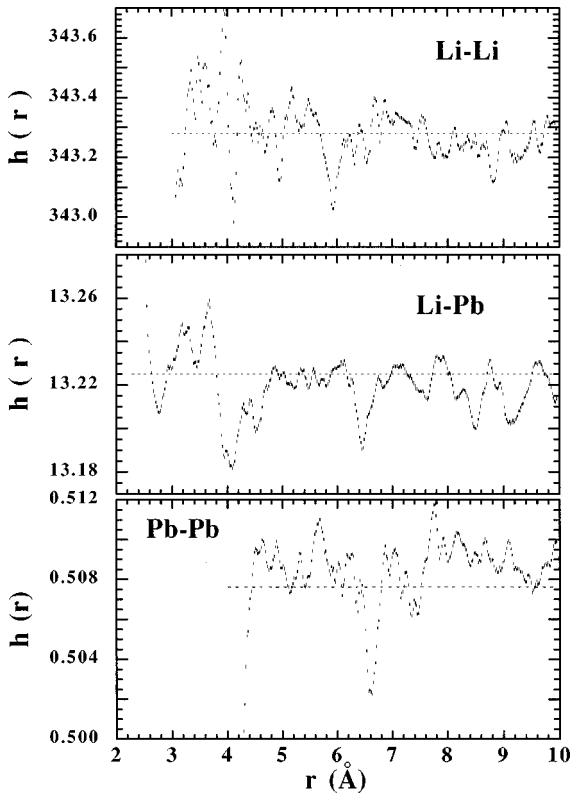

FIG. 4. $h_{\alpha\beta=\mathrm{Li,Pb}}(r)$, kinetic-energy partial correlation functions. Units are (Å ps^{-1})$^{-4}$. The dashed lines show the mean values.

to the numerator of $h(r)$ whereas its influence is strongly felt by the static radial distributions.

A semiquantitative estimate of the spatial extent of the vibrations is provided by inspection of the decay of oscillation in $h_{\alpha\beta}(r)$. Curiously enough, the $h_{\mathrm{LiLi}}(r)$ shows the strongest attenuation with distance, indicating that motions of particles separated by distances well above 10 Å would behave as statistically uncorrelated.

The $J_l(\mathbf{Q},E)$ spectra in Fig. 3 show that the departures from the idealized $F23$ structure reported in the crystallographic work [8] also appear in this dynamic quantity. Indeed, the $J_l(\mathbf{Q},E)$ functions depicted in Fig. 3 show a far richer structure than that of the bcc subcell with a two-ion basis mentioned above. The specific crystal symmetry giving rise to such spectra should certainly be lower than $F23$, and the subcells larger than those with 3.5 Å of lattice parameter. This seems definitely required by the rather inhomogeneous distribution of the Pb atoms within the Li lattice which, in certain respects, is reminiscent of a layered system where some of the layers with high-Pb content alternate with others depleted in the heavy element. Such an alternating-layer structure seems then to be the most plausible candidate offering an explanation for the rich spectral shape. Indeed, the microscopic dynamics within each layer do have to be remarkably different, which would translate into different spectra and therefore this may well be the cause of the large anisotropy shown by excitations depicted in Fig. 3.

C. Collective dynamics: Effects of orientational averaging

To allow direct contact with measurements carried in the molten state (or in polycrystal samples), a powder averaged $\langle S(Q,E)\rangle_\theta$ has been calculated by means of sampling over all scattering directions $\mathbf{Q}$ having the same wave-vector moduli. The process was then carried out in a way mimicking Ref. [20] and some specific examples are shown in Fig. 5. The most glaring result after comparing those graphs with others shown in Fig. 3 corresponding to specific crystal directions concerns the very strong effects that orientational averaging has on an experimentally accessible quantity such as $S(\mathbf{Q},E)$ for a solid showing excitation branches of very different frequencies in neighboring Brillouin zones. As can easily be seen, a very strong dependence with wave vector is now apparent for both the low- and high-frequency bands. Such a remarkable effect obviously arises from orientationally averaging spectra such those of Fig. 3 which show a strong dependence of the intensity of the different components of its multiplet structure which, on the other hand, show very little dispersion.

Additional information on the structure of the low-frequency band is also provided by examination of the $\langle S_{ij}(Q,E)\rangle_\theta$ partial spectra for Li-Li, Li-Pb, and Pb-Pb correlations. This is so since the integrated intensity of a phonon band dominated by acoustic modes should be such that [21]

$$\int dE\langle S_{ij}(Q,E)\rangle_\theta \propto \exp(-2W_Q)Q^2\langle|F(\mathbf{Q})|^2\rangle_\theta \times\sum_{\mathbf{q}}\sum_j \frac{k_BT}{\omega_{\mathbf{q}}^{j2}}\frac{\langle\mathbf{Q}\cdot\boldsymbol{\sigma}_{\mathbf{q}}^j\rangle_\theta}{2M^{1/2}}, \qquad (6)$$

where the exponential is the Debye-Waller factor, $F(\mathbf{Q})$ is the structure factor for the unit cell, the first sum runs over those phonon wave vectors $\mathbf{q}$ which are characteristic of longitudinal excitations with frequencies $\omega_{\mathbf{q}}^j = c_s^j\mathbf{Q}$, and the second runs over the number of modes. The quantity $\boldsymbol{\sigma}_{\mathbf{q}}^j$ stands for the phonon polarization vector and the angular brackets denote a powder average. Since we are dealing with the low-frequency spectrum of a polycrystalline cubic solid the mode eigenvectors should correspond to those of traveling plane waves defined in terms of an angle between the phonon wave vector and the direction of propagation. Following the line of reasoning described in Ref. [22] concerning the relevant averages to be taken one arrives at the result

$$\int dE\langle S_{ij}(Q,E)\rangle_\theta \propto \exp(-2W_Q)\frac{Q^2k_BT}{2M} \times\int d\omega\frac{q_l^2}{c_s\omega}\int_{-1}^{1}d\mu\mu^2S \times(\sqrt{Q^2+q_l^2-2Qq_j\mu}), \qquad (7)$$

where $q_l=\omega/c_s$, and q_j is the phonon wave vector at a given Q and is chosen in a way such that the three quantities within the square root define a triangle. Equation (7) thus shows that the nontrivial factors governing the intensity of a crystal excitation are the Debye-Waller term, the inverse of the frequency, and the integral taken over the static structure factor $S(Q)$. For the values of the momentum transfer and temperatures of our concern, the first contribution can be disregarded since it amounts to a uniform decrease of the intensity with increasing Q. Equation (7) thus predicts that for

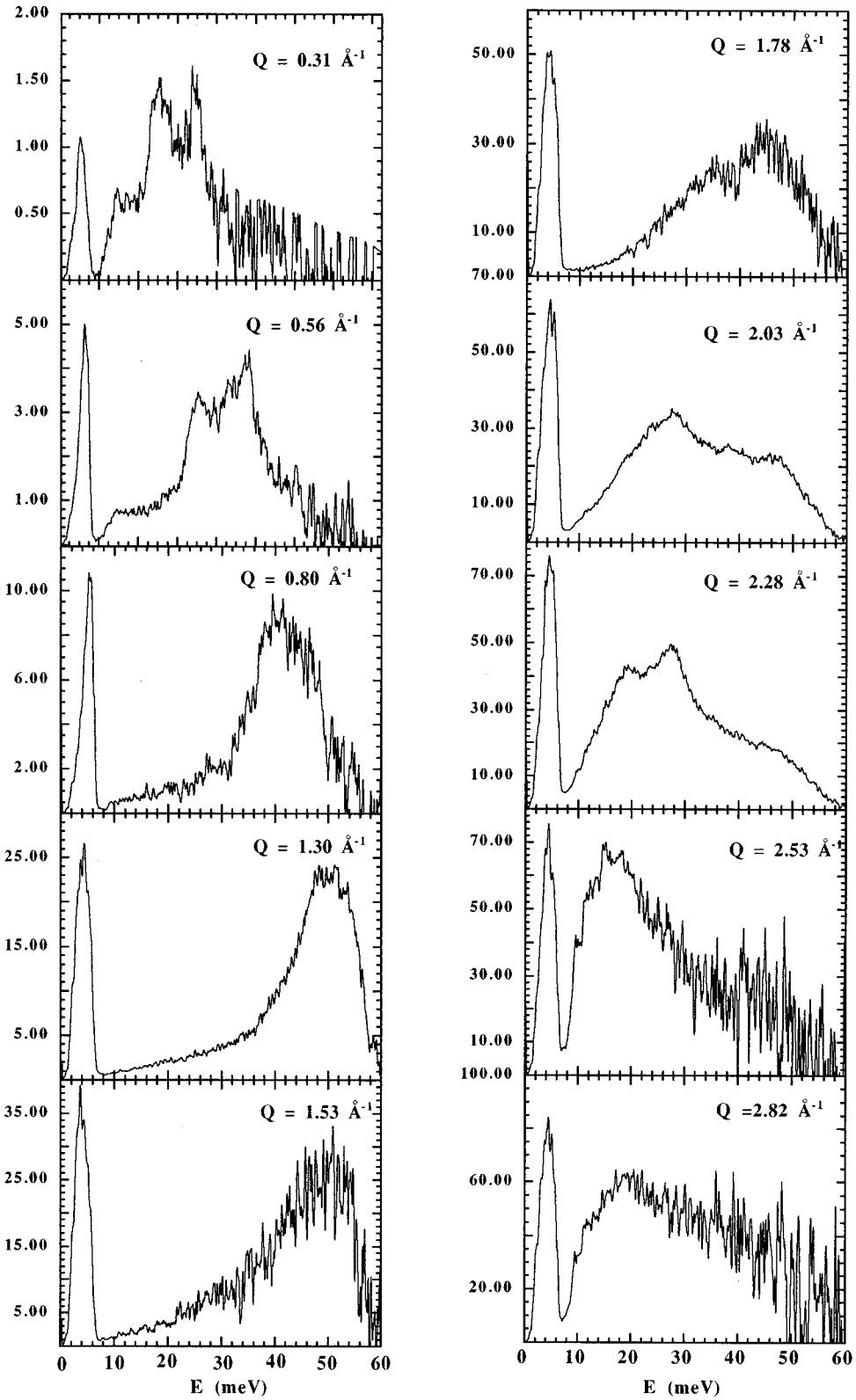

FIG. 5. A sample of $\langle S(Q,E)\rangle_\theta$ polycrystalline averaged spectra. The corresponding momentum transfers are shown as insets.

excitations of longitudinal-acoustic origin one should observe a momentum-transfer dependence of their intensities which show the same modulation as the measured polycrystalline Bragg pattern.

A comparison of the behavior expected on the basis of the above paragraph and the results concerning the partial dynamic structure factors at low frequencies is enabled by inspection of Fig. 6.

The first observation worth noting concerns the presence of a well defined band extending up to about 7 meV in the three partial spectra, showing basically the same extrema and a width which remains fairly constant (they would be ex-

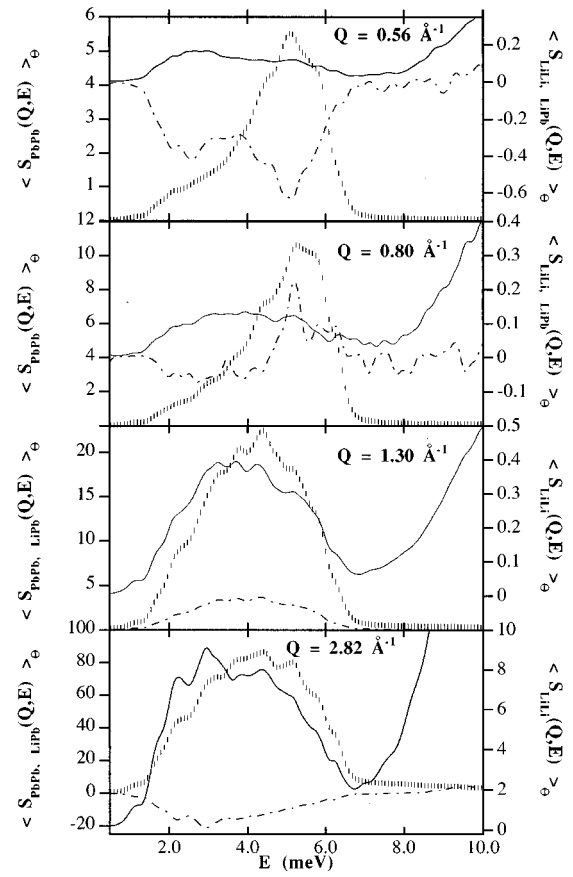

FIG. 6. Low-frequency region of the partial $\langle S_{ij}(Q,E)\rangle_\theta$ spectra. Solid lines depict the $\langle S_{\mathrm{LiLi}}(Q,E)\rangle_\theta$, bars $\langle S_{\mathrm{PbPb}}(Q,E)\rangle_\theta$, and dot-dashes show the $\langle S_{\mathrm{LiPb}}(Q,E)\rangle_\theta$ cross correlation. The corresponding momentum transfers are shown as insets.

pected to increase $\propto Q^2$ at low wave vectors if such bands corresponded to a unique excitation). The intensity turns out to be negative for the Li-Pb correlation at low wave vectors due to the negative scattering length on ^{7}Li (i.e., the correlation is positive at low wave vectors and turns into negative values at larger Q values).

Second, the spectra for Li-Pb cross correlations show a strong wave-vector dependence in their phase. It starts as a negative band at the lowest wave vector, splits into a negative lobe below 4 meV and a positive peak at about 5 meV for $Q=0.8$ Å^{-1}, becomes a positive band from about 1 Å^{-1} up to $Q=2.2$ Å^{-1}, and again, turns back to negative for $Q=2.5$–2.8 Å^{-1}. This behavior runs entirely counter to that describable for an acoustic excitation by Eq. (7) and therefore it shows that the Li-Pb spectra are composed of at least two bands having rather different characters.

Finally and following what has been written above, the three partial spectra show, at wave vectors below 0.8 Å^{-1}, the presence of at least two groups of excitations. The Li-Pb and Li-Li correlations clearly show two peaks with maxima ≈ 2–2.5 meV and ≈ 5 meV at the lowest explored wave vectors. Because of the behavior mentioned in the preceding paragraph, the band centered at about 5 meV cannot be dominated by excitations of acoustic character.

The observations listed above thus reveal the contribution of opticlike modes to the low-frequency band. Their character cannot be ascertained in full but, in view of the large atomic mean-square displacements found for the Pb, they can be thought of as some sort of ''resonant'' modes [15]. Also, the implication of the facts given above is that purely acoustic dispersions thus have to be bounded below 4 meV.

IV. DISCUSSION

The presence of an excitation in binary fluid (or dense-liquid) mixtures of disparate-mass particles which shows an apparent phase velocity close to that of the pure, light component has been verified experimentally [4,7,23], and its origin is understood on the basis of the revised Enskog theory for hard spheres [6]. The results of such calculations are often displayed as wave-vector-dependent eigenvalues corresponding to sound propagation, mass, and thermal diffusions [6,17], as well as other eigenmodes referred to as ''kinetic modes,'' that is, those whose range of existence is limited to the kinetic regime that is beyond the hydrodynamics realm (typically for wave vectors above 5×10^{-3} Å^{-1}). In all cases, it is found that the real part of the frequency of the kinetic modes ω_Q vanishes when the hydrodynamic regime is approached, whereas their damping coefficients Γ_Q (basically an inverse of the peak width) retain finite values as $Q\rightarrow 0$. An exercise worth undertaking would be to consider the renormalized excitation frequencies $\Omega_Q=\sqrt{\omega_Q^2+\Gamma_Q^2}$ instead of the ''bare'' quantities ω_Q as the physically meaningful frequencies. The rationale behind this is to treat the damping coefficient as a ''dressing'' term to be added to the ω_Q interaction-free frequency on the same footing as any additional anharmonic frequency shift [24]. In addition, for well defined excitations corresponding to isolated peaks in the spectrum, the frequencies Ω_Q now correspond to those of maxima of peaks in $J_l(Q,E)$. If such a transformation were applied to the calculated data [6] then one would find that the hydrodynamic $Q\rightarrow 0$ limits of the ''kinetic modes'' correspond to finite frequencies rather than to the usual linear dispersion expected for sound modes.

On experimental grounds [4], the frequencies plotted as ''dispersion relations'' for molten Li_4Pb can be identified with those Ω_Q which represent the natural frequency of an oscillator with damping constant Γ_Q. From here a connection between the experimental [4] and simulation [5] data for the melt with the present result is clearly envisaged. Figure 7 shows a comparison of frequencies derived from experimental means with those corresponding to maxima of the most prominent peaks in spectra such as those shown in Fig. 5. A glance at the graph shown in Fig. 7(b) reveals that the shape of the ''dispersion curve'' followed by the experimental points is basically identical to that defined by the Q dependence of the frequencies of the most intense peak in $\langle S(Q,E)\rangle_\theta$. As expected, the frequencies of the crystal spectra at $T=64$ K are significantly higher than those of the liquid at $T=1075$ K, a fact easily understandable by consideration of the thermal expansion and concomitant force-constant softening reported for pure Li [13]. A point also worth making is the fact that data for both the crystal and melt lie substantially above the hydrodynamic $\omega_Q=c_sQ$ law calculated from the macroscopic sound velocity of pure Li.

In contrast, a well defined ''dispersion relation'' that is the kind of behavior one would expect to find for the spec-

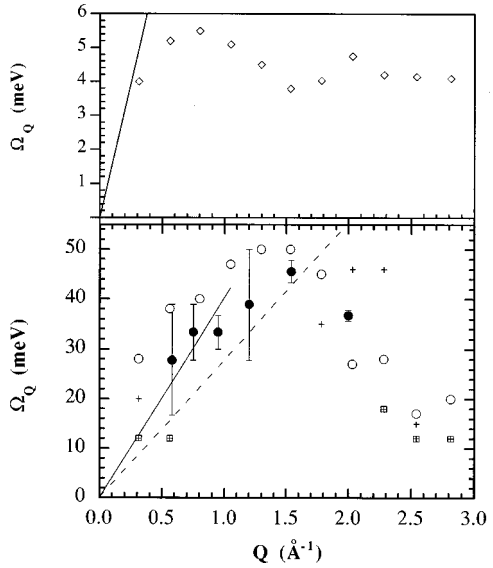

FIG. 7. (a) The wave-vector dependence of the peak centroid of the low-frequency band of spectra like those $\langle S(Q,E)\rangle_\theta$ shown in Fig. 5. The straight line corresponds to the dispersion of hydrodynamic phonons traveling with a phase velocity of 2500 m/s. (b) Experimental frequencies for the molten alloy (filled symbols with error bars) [4], those corresponding to the maxima of the most intense peak of the $\langle S(Q,E)\rangle_\theta$ polycrystalline averaged spectra (open circles), and maxima of less intense peaks are displayed by crosses and squares. The solid and dashed straight lines correspond to the hydrodynamic dispersion of waves traveling with the phase velocity of pure fcc Li and molten Li metal, respectively.

trum of a polycrystalline cubic solid [20] is here encountered for the wave-vector dependence of the peak centroid of the low-frequency band, as shown in Fig. 7(a). The Ω_Q frequencies corresponding to such a band describe a curve showing a maximum at about 0.8 Å^{-1} at a frequency of about 5.5 meV, a minimum at about 1.8 Å^{-1} and at $Q\rightarrow 0$ they seem to approach the hydrodynamic dispersion corresponding to the averaged longitudinal sound velocity of the crystal [25]. As shown by the spectral distribution, such low-frequency peaks arise from the motions of *both* light and heavy particles and therefore they comprise all those modes involving the propagation of sound.

As far as the remarkably short lifetime of the high-frequency modes, our present result for the crystal as well as previous findings for the melt [4,5] can be rationalized on the basis of some analytical results derived some time ago [26] for the approximate calculation of spectra for heavily (isotopic) disordered crystals. There [26] it is found that the damping coefficient for a normal mode of frequency ω_Q would in our case would be given by

$$\Gamma_Q=\frac{\epsilon^2\omega_Q^2}{2\sqrt{(\omega_L^2-\omega_Q^2)}},\quad \epsilon^2=p(1-p)M^2\left(\frac{M_{\mathrm{Pb}}-M_{\mathrm{Li}}}{M_{\mathrm{Pb}}M_{\mathrm{Li}}}\right)^2, \tag{8}$$

with $M=pM_{\mathrm{Li}}+(1-p)M_{\mathrm{Pb}}$, $p=22/27$ (the probability of a light particle of mass M_{Li} to be present at a given site), and ω_L stands for the maximum frequency for a lattice made up of light atoms only. A glance at Eq. (8) reveals that the higher the mode frequency, the shorter the lifetime whereas low-frequency, long wavelength modes decay far slower. Also, the larger the mass difference between the particles composing the crystal the larger the damping coefficient. Under these conditions one expects that waves of such high frequencies will be heavily damped after times comparable to those required to travel distances as short as one lattice spacing. The result is reminiscent of that reported by Rubin [27] on the energy flow in binary crystals with moderate mass ratios, where it was shown that local temperature disturbances will last for times which are long compared with that required for a sound wave to travel one lattice spacing [27]. In consequence, such high-frequency excitations will contribute little to heat or momentum-transport processes.

As far as long-wavelength acoustic waves are concerned, the crystal should be better regarded as a continuous medium with a mass density given by an average such as M. Sound velocities are then inversely proportional to $\sqrt{M}$ and therefore the presence of particles with disparate masses in different concentrations will only play the role of varying the mass density and thus the macroscopic values for the sound velocities.

Finally, a fact which also seems worth commenting on regards the appearance of nonacoustic components within the low-frequency band showing frequencies as low as 4–5 meV as depicted in Fig. 6. Such a phenomenon is now understood in crystals having finite concentrations of (i.e., not isolated) ''defects'' [28]. A well known example of this is the appearance of low-frequency optical phonon branches in metal hydrides out of a host lattice showing acoustic modes only [29]. The mechanism leading to the emergence of such a new branch involves the coupling of long-wavelength phonons to ''resonance'' modes involving the heavy particles. Low ''defect'' concentrations will lead to changes in the linewidth and a small shift of the host-lattice phonons only, whereas hybridization of the phonon and ''resonance'' modes is expected for higher concentrations. Under such circumstances the acoustic dispersions split into an optic and an acoustic branch which is now confined to frequencies below the former.

V. CONCLUSIONS

Our present results concern the dynamics of a system amenable to experiment having characteristics (i.e., mass ratio) akin to that recently described in [30]. Such a conceptual device, which is formed by Lennard-Jones particles mimicking argon but having a mass ratio $R=30$, shows a phenomenology close to that described here. The findings also lend support to the conjecture stated by Campa and Cohen [6] regarding the possibility of detecting the presence of the ''kinetic modes'' even if the fluid supporting them undergoes a freezing transition. The computation of crystal spectra along the main symmetry directions as well as comparison of such spectra with the orientationally averaged quantities served to disentangle the mechanism by which the steeply dispersive ''kinetic modes'' appear in a fluid. Here, it is shown that it arises as a consequence of orientationally averaging over Brillouin zones having dispersion branches appearing at substantially different frequencies. In other words, the results validate the inference made in Ref. [6] on the applicability of

the revised Enskog theory to a crystalline material. That is, it can be used to predict the main features of the spectra of a polycrystalline sample but the identification of the calculated eigenvalues with physical frequencies characteristic of sound propagation cannot be made. The validity of the latter conclusion is not limited to binary mixtures but should be applicable to cases such as those concerning molecular materials where rather similar phenomena have been reported [31].

ACKNOWLEDGMENT

This work was performed in part under DGICYT (Spain) Grant No. PB95-0072-C03-01.

[1] A.A. Maradudin, E.W. Montroll, G.H. Weiss, and I.P. Ipatova, *Theory of Lattice Dynamics in the Harmonic Approximation*, 2nd ed. (Academic Press, New York, 1971), Chap. 8, p. 353; also see I.M. Lifshits, S.A. Gredeskul, and L.A. Pastur, *Introduction to the Theory of Disordered Systems* (Wiley, New York, 1988), Chap. 6, p. 314.

[2] S.W. Lovesey, *Theory of Neutron Scattering from Condensed Matter* (Oxford Science Publications, Oxford, 1986), Vol.1, p. 150.

[3] W.A. Kamitakahara and J.R.D. Copley, Phys. Rev. B **18**, 3772 (1978).

[4] M. Alvarez, F.J. Bermejo, P. Verkerk, and B. Roessli, Phys. Rev. Lett. **80**, 2141 (1998).

[5] R. Fernández-Perea, M. Alvarez, F.J. Bermejo, P. Verkerk, B. Roessli, and E. Enciso, Phys. Rev. E **58**, 4568 (1998).

[6] A. Campa and E.G.D. Cohen, Phys. Rev. A **41**, 5451 (1990).

[7] P.H.K. de Jong, P. Verkerk, C.F. de Vroege, L.A. de Graaf, W.S. Howells, and S.M. Bennington, J. Phys.: Condens. Matter **6**, L681 (1994).

[8] A. Zalkin and W.J. Ramsey, J. Phys. Chem. **62**, 689 (1958).

[9] G. Grube and H. Klaiber, Z. Elektrochem. **40**, 745 (1934).

[10] A. Zalkin and W.J. Ramsey, J. Phys. Chem. **60**, 234 (1956); **60**, 1275 (1956).

[11] A.P. Copestake, R. Evans, H. Ruppersberg, and W. Schirmacher, J. Phys. F **13**, 1993 (1983).

[12] G. Jacucci, M. Ronchetti, and W. Schirmacher, in *Condensed Matter Research Using Neutrons*, edited by S.W. Lovesey *et al.* (Plenum Press, New York, 1986), p. 139; J. Bosse, G. Jacucci, M. Ronchetti, and M. Schirmacher, Phys. Rev. Lett. **57**, 3277 (1986).

[13] M.M. Beg and M. Nielsen, Phys. Rev. B **14**, 4266 (1976).

[14] M. Rovere and M.P. Tosi, Rep. Prog. Phys. **49**, 1001 (1986).

[15] P.H. Dederichs, C. Lehmann, H.R. Schober, A. Scholz, and R. Zeller, J. Nuclear Mater. **69-70**, 176 (1978).

[16] J.P. Boon and S. Yip, *Molecular Hydrodynamics* (McGraw-Hill, New York, 1980), p. 187.

[17] I.M. de Schepper and E.G.D. Cohen, J. Stat. Phys. **27**, 223 (1982).

[18] E. Burkel, *Inelastic Scattering of X-rays with Very High Energy-Resolution* (Springer, Berlin, 1991); for simulations see also A. Torcini, U. Balucani, P.H.K. de Jong, and P. Verkerk, Phys. Rev. E **51**, 3126 (1995).

[19] S.R. Nagel, A. Rahman, and G.S. Grest, Phys. Rev. Lett. **47**, 1665 (1981).

[20] F.W. de Wette and A. Rahman, Phys. Rev. **176**, 784 (1968).

[21] In S.W. Lovesey, Ref. [2], p.119.

[22] J.M. Carpenter and C.A. Pelizzari, Phys. Rev. B **12**, 2391 (1975).

[23] W. Montfroij, P. Westerhuijs, and I.M de Schepper, Phys. Rev. Lett. **63**, 544 (1989); G.H. Wegdam, A. Bot, R.P.C. Schram, and H.M. Schaink, *ibid.* **63**, 2697 (1989).

[24] Some useful remarks about the meaning of fit parameters arising from the use of the damped harmonic oscillator function are given in H.R. Glyde, *Excitations in Liquid and Solid Helium* (Clarendon Press, Oxford, 1994), pp.184 and 185.

[25] Computed using an average over the elastic constants as derived from the excitation phase velocities computed using low-Q data for the three principal crystal symmetry directions.

[26] From Maradudin *et al.* in Ref. [1], p. 662.

[27] R.J. Rubin, Phys. Rev. **131**, 964 (1963).

[28] H.R. Schober, in *Physics of Phonons*, edited by T. Paskiewicz, Springer Lecture Notes in Physics Vol. 285 (Springer, Berlin, 1987), p. 197.

[29] See for instance, S.M. Shapiro, D. Richter, Y. Noda, and H. Birnbaum, Phys. Rev. B **23**, 1594 (1981).

[30] E. Enciso, N.G. Almarza, M.A. Gonzalez, F.J. Bermejo, R. Fernández-Perea, and F. Bresme, Phys. Rev. Lett. **81**, 4432 (1998).

[31] See, for instance, F.J. Bermejo, M. Alvarez, R. Vallauri, and S.M. Bennington, Phys. Rev. E **51**, 2250 (1995), and references therein.